Intermediate 4*f* bonding structure for samarium under pressure

Y. C. Zhao,* F. Porsch, and W. B. Holzapfel
Fachbereich Physik, Universität-GH-Paderborn, D-33095 Paderborn, Germany
(Received 31 March 1994; revised manuscript received 6 June 1994)

The crystal structure of the low-symmetry phase Sm(V) was studied by synchrotron x-ray diffraction under isothermal compression at room temperature up to 77 GPa (volume fraction=0.45). Measured lattice spacings and diffraction intensities for Sm(V) in the pressure range beyond the phase mixing show that this phase can be identified as a prototype structure with 3 atoms in the hexagonal unit cell. The occurrence of this low-symmetry structure gives strong evidence for a rapid increase of 4*f*-electron bonding in Sm in the pressure range above 37 GPa.

I. INTRODUCTION

It is well known that regular trivalent lanthanide metals from lanthanum to lutetium, but without cerium, europium and ytterbium, show a systematic sequence of phase transitions under pressure in the direction: hcp→Sm-type→dhcp→fcc→distorted fcc.[1-7] This sequence has been related to an increasing *d* character of the conduction band under compression.[8,9] With Pearson's short notation[10] for structure types, this sequence can be denoted also as $hP2 \rightarrow hR9 \rightarrow hP4 \rightarrow cF4$. A recent study on the structure of the distorted-fcc phase for Pr resulted in an assignment of this phase as a rhombohedral structure with space group $R\bar{3}m$ and structure type $hR24$.[11] In addition, low-symmetry structures have been observed not only in cerium[12] and praseodymium[13] under pressure but also in neodymium and samarium[14] and it was argued, that these structures are related to the beginning of *f* bonding under pressure in these elements.[4,6] Since the initial observation of a low-symmetry phase in Sm was based only on measurements over a limited range in pressure for the new phase, the tentative assignment of a monoclinic structure[5,6] was considered just as a provisional indexing scheme requiring further experimental or theoretical support. A later study[15] by the same energy-dispersive diffraction techniques, however, over a more extended region in pressure up to 100 GPa did not resolve the structural problem but rather used two different indexing schemes for the low-symmetry phase Sm(V) above 32 GPa. The most recent study[16] up to 189 GPa reported in addition one further phase transition at 91 GPa into a body-centered tetragonal ($tI2$) structure, denoted Sm(VI), without any further result on the intermediate (low-symmetry) phase Sm(V). Thus, further experimental work seemed to be necessary to resolve the structure of this intermediate phase.

II. EXPERIMENTAL

The present experiments were carried out with energy-dispersive x-ray diffraction (EDXRD) using synchrotron radiation at HASYLAB, DESY (Hamburg). The details of this experimental station have been described previously.[17] High pressure was generated with beveled anvils in a diamond-anvil cell[18,19] (DAC). Inconel gaskets with a 100-μm diam hole were used. Mineral oil (dehydrated with Rb metal) served as pressure transmitting medium and prevented oxidation of the sample during sample loading. The collimator in front of the DAC was set to 60×60 μm^2, sometimes to 20×20 μm^2. Fine ruby powder was loaded in the DAC as pressure sensor and the nonlinear ruby luminescence scale[20] was adopted for the pressure determination. The Sm sample material was provided by K. A. Gschneidner, Jr., with chemical analysis giving the major impurity contents in atomic ppm as follows: 310 for oxygen, 545 for hydrogen, and 25 for all other lanthanides. Two independent runs of x-ray-diffraction experiments were performed in the present study with reproducible results.

In the evaluation of overlapping peaks, the restricted resolution of the energy-dispersive technique can result in different limitations than that of angular-dispersive experiments. With the present experimental conditions, the resolution $d/\Delta d$ for *d* spacings increases typically from 70 to 110 in the range of *d* from 250 to 100 pm as discussed in previous publications on this technique.[17] However, due to the well-known (Gaussian) peak shape, profile fitting can resolve overlapping peaks even with 10 times higher resolution. On the other hand, under pressure the common deviatoric stresses and slight pressure inhomogeneities lead finally to almost the same resolution in this technique as in angular-dispersive measurements on samples under similar conditions.

III. RESULTS

Typical spectra for regions of pure Sm(IV) and Sm(V) are shown in Fig. 1. Least-squares fits of Gaussian lines to the observed peaks in the diffraction spectra result in the *d* values presented in Fig. 2 for the pressure range of the phases Sm(IV) and Sm(V). It can be noticed in this figure that the region of phase mixing extends with increasing pressure from 39 to 46 GPa. On decompression the mixing of Sm(IV) and Sm(V) starts at 35 GPa. The present best estimate for the equilibrium transition pressure between the Sm(IV) to Sm(V) is therefore 37(4) GPa. Only above 46 GPa the peaks of Sm(IV) are sufficiently suppressed to allow for an unambiguous assignment of

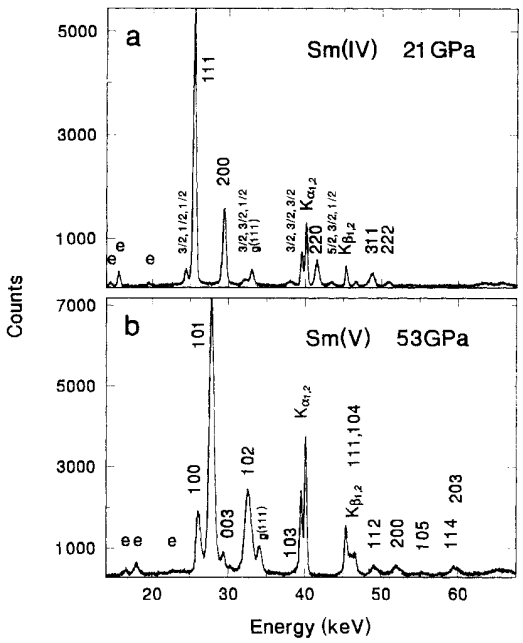

FIG. 1. Diffraction spectra of Sm(IV) (a) and Sm(V) (b). "*e*" represents an escape peak. "*g*" represents a gasket diffraction. For the indexing, see the text.

the new structure for Sm(V). The spectrum of Sm(V) is indexed according to a primitive hexagonal structure $hP3$, whereas fractional Miller indices for the superlattice reflections of a fcc superstructure are used for the indexing of the spectrum for Sm(IV) with its "distorted-fcc" structure.

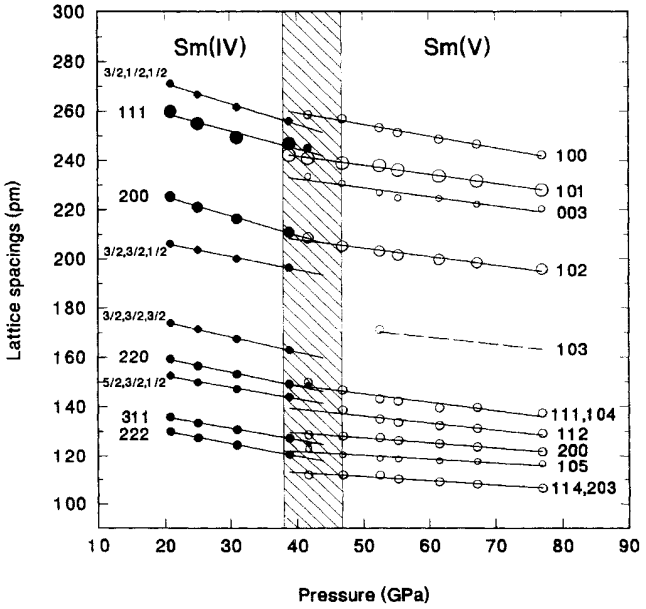

FIG. 2. Variation of lattice spacings for the observed diffraction peaks with increasing pressure. Solid circles and open circles represent Sm(IV) and Sm(V), respectively. The region of phase mixing is denoted by hatched area. The (103) diffractions from Sm(V) [see Fig. 1(b)] overlap with the K_α doublet.

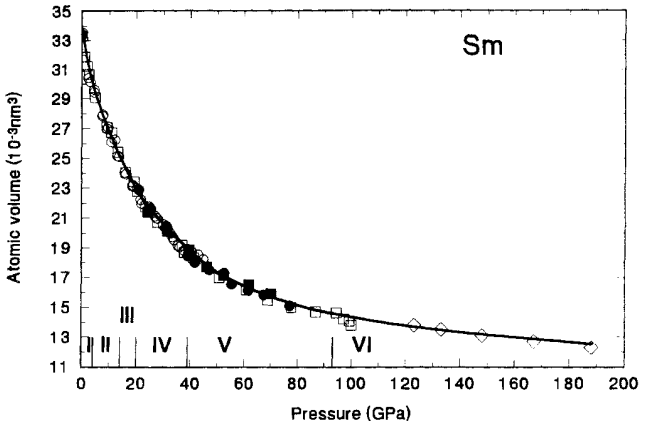

FIG. 3. Pressure-volume relation for Sm up to 189 GPa. Open circles, open squares, and open diamonds are data taken from Refs. 5, 15, and 16, respectively. The V/V_0 data from Refs. 15 and 16 are converted to atomic volume V in the present plot using $V_0 = 33.21 \times 10^6$ pm^3 per atom. The solid symbols are data of the present study with circles and squares representing two different samples. The solid curve is a fit of a third order Birch EOS to the data.

The problems in assigning a specific structure to experimental data for the distorted-fcc regions of the lanthanide metals are not trivial and will be discussed in detail later.[21] Because the distortions are small, the data for the atomic volume of Sm(IV) can be evaluated equally well on the basis of the fcc assignment. The corresponding values for the atomic volume at different pressures and ambient temperature are represented together with previous data from the literature[5] in Fig. 3, which shows, in general, good agreement between the previous and present results.

The beginning of the Sm(IV)→Sm(V) phase transition is heralded by the growth of a new peak on the low-energy side of the (111) fcc peak in the Sm(IV) pattern. After completion of this phase transition at pressures above 46 GPa, the diffraction patterns for pure Sm(V) become rather simple and a primitive hexagonal lattice ($hP3$) with three atoms in the unit cell gives excellent agreement between observed and calculated d spacings as shown in Table I for one typical pattern. Furthermore, the evaluation of the lattice parameters, as shown in Fig. 4, results in an atomic volume, shown also in Fig. 3, which corresponds to an almost continuous extrapolation of the data from the lower pressure phases with a possible volume discontinuity smaller than 1%.

Since the observed c/a ratio for Sm(V) with the constant value of 2.36(3) deviates only slightly from the "ideal" value 2.45 of an fcc lattice in trigonal representation, a slight trigonal distortion of a fcc lattice can be taken as starting point in a structural refinement for this phase. The occurrence of (100) diffraction indicates that Sm(V) cannot have rhombohedral symmetry. In addition, the diffraction spectra of Sm(V) show that diffractions with $(00l)$ occur only when $l = 3n$ (n is integer). This suggests that at least a 3_1 or 3_2 axis is present. Hence one may start characterizing the crystal structure of Sm(V) with the space group for $P3_1$ or its

TABLE I. The indexing of the Sm(V) diffraction pattern at 77 GPa using a hexagonal cell with $a=280.6$ pm and $c=664.8$ pm. d_{obs} and d_{calc} represent the observed and calculated lattice spacings, respectively.

d_{obs} (pm)	d_{calc} (pm)	hkl
242.2	243.0	100
227.9	228.2	101
220.5	221.4	003
195.8	196.1	102
(190.5)		gasket(111)
137.3	137.3	111
	137.2	104
129.1	129.2	112
121.7	121.5	200
116.7	116.6	105
	107.1	114
106.5	106.5	203

enantiomorphic space group $P3_2$ with three atoms occupying the $3a$ position, which can be rewritten as $[-(1+2\delta_a-\delta_b)/3,-(1+\delta_a+\delta_b)/3,0]$; $[2(1+\delta_a+\delta_b)/3,-(\delta_a-2\delta_b)/3,\frac{1}{3}]$; $[(\delta_a-2\delta_b)/3,(1+2\delta_a-\delta_b)/3,\frac{2}{3}]$, where δ_a and δ_b are the deviations of atomic positions, along the two axes of the hexagonal basal plane. $\delta_a=\delta_b=0$ and $c/a=2.45$ represent the fcc structure. When intensities of EDXRD spectra for Sm(V) are calculated by sampling δ_a and δ_b in $|\delta_a|\leq\frac{2}{3}$ and $|\delta_b|\leq\frac{2}{3}$, only $\delta_a/2=\delta_b$ gives satisfactory results for calculated and observed intensities of the EDXRD spectra. Figure 5(b) shows the calculated intensities for Sm(V) at 77 GPa with $\delta_a/2=\delta_b=0.12$. In this case the symmetry of this phase

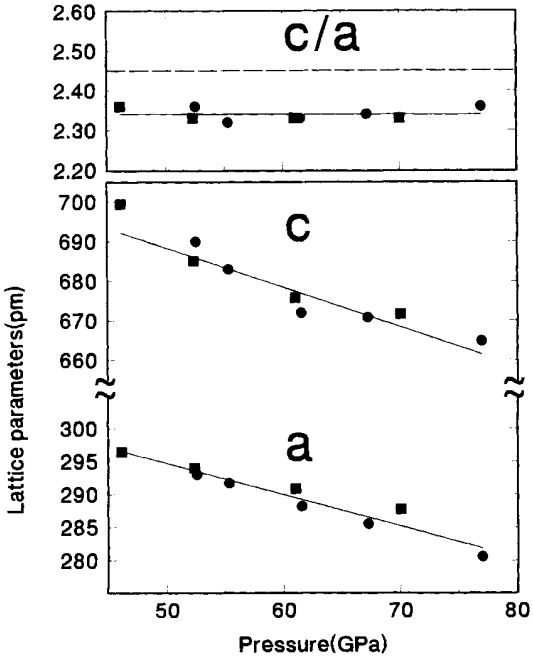

FIG. 4. Effect of pressure on the lattice parameters and the c/a ratio for Sm(V). The circles and squares represent two independent runs of experiments (i.e., two different samples). The dashed line represents the c/a value for a fcc structure.

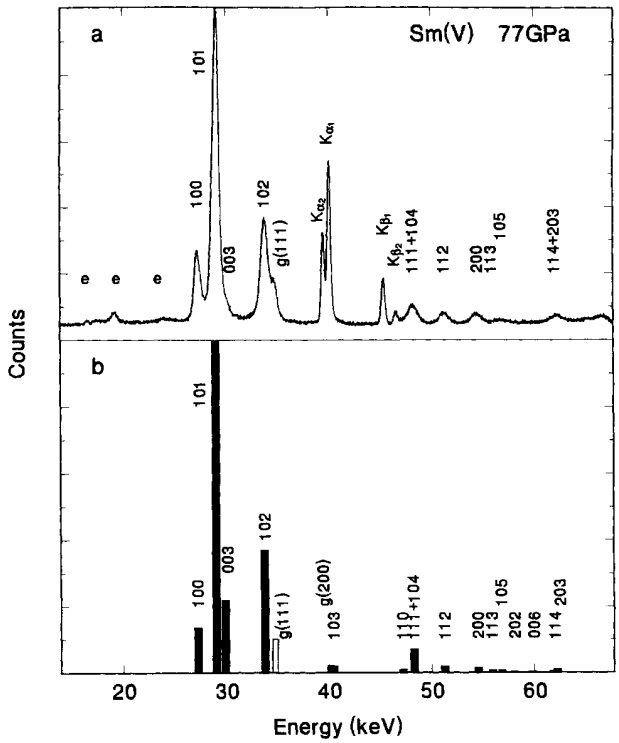

FIG. 5. Observed (a) and calculated (b) EDXRD spectrum for Sm(V) at 77 GPa. "e" represents an escape peak. "g" represents a gasket diffraction.

corresponds to a pair of enantiomorphic space groups $P3_121$ or $P3_221$. It should be noted that in the intensity of each peak shown in Fig. 5(b) is the sum of all the allowed $\{hkl\}$ and $\{hk\bar{l}\}$ reflections although only (hkl) indexing is given in the figure. The calculated intensities are in reasonable agreement with the observed values. Only the intensity of the (003) peak is significantly weaker than expected from the calculation, however, such difference seems to be typical in high-pressure studies for reflections with low multiplicities due to texture.[5,6] Within the experimental accuracy both δ_a and δ_b as well as c/a show no systematic variation in the whole stability range for Sm(V). Figure 6 illustrates the proposed crystal structure for Sm(V) together with a view of the atomic arrangement along the c axis. The atomic positions are A:$(-u,-u,0)$, B:$(u,0,\frac{1}{3})$, and C:$(0,u,\frac{2}{3})$, where $u=\frac{1}{3}+\delta_b=0.45$. It can be noticed that this structure is isopuntal with $hP3$-Se(I), the structure of α-Se. However, the atomic position parameter u in the $hP3$-Se(I) structure shows just the opposite sign in δ_b than in the present $hP3$-Sm(V) structure. One may thus consider the structure of Sm(V) indeed as a new structural prototype for metallic elements with very specific features in their bonding properties. In contrast to the helical chains of short covalent bonds in the $hP3$-Se(I) structure, the $hP3$-Sm(V) structure is characterized by open channels along the c axis at the location of these chains in $hP3$-Se(I). In addition a fourfold nearest-neighbor coordination is observed in Sm(V) in contrast to the twofold coordination

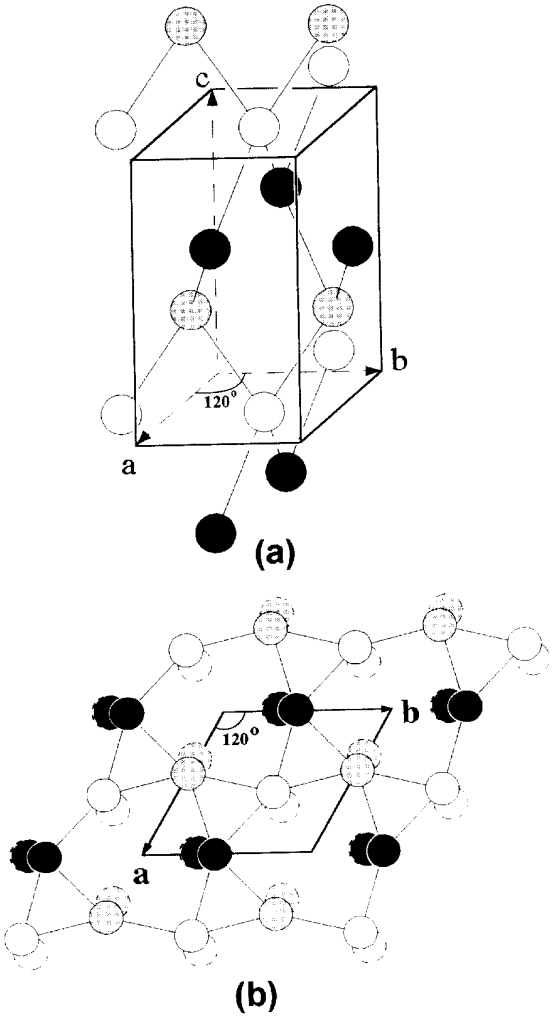

FIG. 6. Crystal structure of Sm(V) (a) and atomic arrangement projected along the c axis (b). White, gray, and black balls represent $z=0$, $\frac{1}{3}$, and $\frac{2}{3}$, respectively. In (b) the balls with dashed rim represent the fcc positions. The hexagonal unit cell is represented by thick lines and the bonds among the nearest neighbors are shown by thin lines.

of $hP3$-Se(I). Moreover, for both $hP3$-Se(I) and $hP3$-Te(I), which is also commonly denoted α-Te, the c/a values vary with pressure from 1.13 to 1.37 and 1.33 to 1.43, respectively,[22] while $c/a=2.36$ for $hP3$-Sm(V) remains constant and much closer to the ideal fcc value of 2.45.

Since both structures Sm(IV) ("distorted-fcc") as well as $hP3$-Sm(V) are closely related to the highly symmetric fcc structure realized in $cF4$-Sm(III), a comparison of the diffraction pattern among these three different structures seems to be appropriate at this point as illustrated in Fig. 7. While the distinction between the structures $cF4$-Sm(III) and Sm(IV) results only from a second-order phase transition with the corresponding appearance of superlattice diffractions and very weak peak splits, second-order phase transitions from Sm(IV) to $hP3$-Sm(V) or from $hP3$-Sm(V) to $cF4$-Sm(III) are not allowed by Landau's theory of phase transition.[21,23,24] Only a first-order distortive (martensitic) phase transition could be imagined corresponding to jumps in both c/a and δ to the values typical for Sm(V) without further variation under pressure. Similarly, the phase transition from Sm(V) to the $tI2$-Sm(VI) can be described only by a path of a first-order distortive transition, which is compatible with the experimental observation that the Sm(V)→Sm(VI) transition has an appreciable hysteresis.[16] In contrast to the case for Sm, for La metal, which has no $4f$ electron, recent studies on its high-pressure structural transition show a reentrant phase transition from the distorted-fcc phase to the fcc phase at about 60 GPa.[25]

IV. DISCUSSION

If one compares the present data for the atomic volume of Sm(IV) and Sm(V) with previous data covering partly an even more extended pressure range[5,15,16] as shown in Fig. 3, one can notice that the present new indexing for the diffraction pattern of Sm(V) does not effect the volume data significantly. Since the last four points from Staun Olsen *et al.*[15] above 90 GPa show a spurious downward variation, due to the fact, that the transition

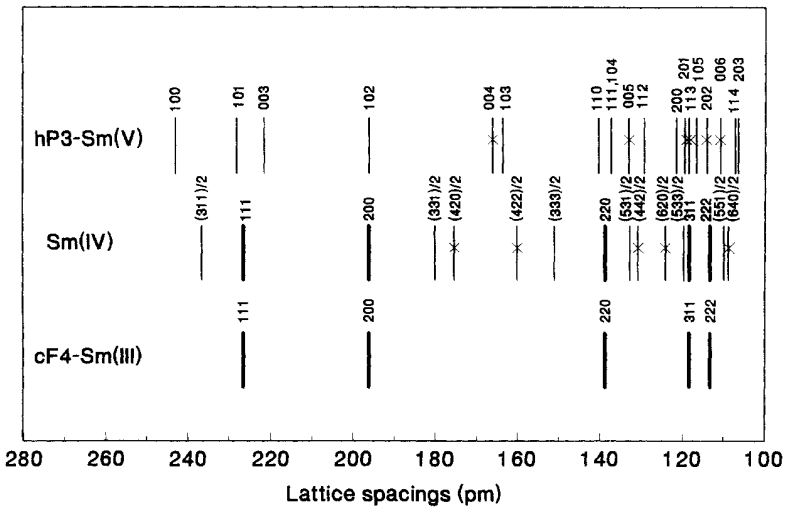

FIG. 7. Illustration of the indexing scheme for $cF4$-Sm(III), "distorted-fcc" Sm(IV) and $hP3$-Sm(V) for the same atomic volume. Thick lines for Sm(IV) represent the strong "fundamental" diffraction peaks. Lines with "x" are not observed due to extinction or possible weak intensities below the present detection limit around 3% of the intensity of the strongest peak.

from Sm(V) to Sm(VI) around 90 GPa was not noticed by these authors, it appears most reasonable to discard these last four data points in the determination of an approximate isothermal (room-temperature) equations of state (EOS) for all the six phases. All the other data follow just one smooth curve within the experimental scatter of ±5% in pressure, and one can fit one common analytical form to all these data. Thereby, possible slight anomalies at the borderlines of the individual phases are obviously suppressed and only a smoothed average relation is obtained. From the many analytical EOS forms found in the literature,[26] only a few are commonly used for solids under strong compression. If one limits the discussion only to second-order forms with the bulk modulus K_0 and its pressure derivative K_0' (both at ambient pressure) as free parameters using the volume at ambient condition V_0 in the relative length $x=(V/V_0)^{1/3}$, the more convenient relations are given by the forms

$$BE2{:}p=\tfrac{3}{2}K_0x^{-7}(1-x^2)[1+c_2(x^{-1}-1)]$$

with $c_2=3(K_0'-4)/4$ for the form derived by Birch from finite strain theory,[27]

$$MV2{:}p=3K_0x^{-2}(1-x)\exp[c_2(1-x)]$$

with $c_2=3(K_0'-1)/2$ for the form derived by Vinet *et al.* from effective potentials,[28] and

$$H12{:}p=3K_0x^{-5}(1-x)\exp[c_{10}(1-x)+c_{12}x(1-x)]$$

with $c_{10}=\ln p_{FG}-\ln(3K_0)$ and $c_{12}=3(K_0'-3)/2-c_{10}$ derived more recently[29] by interpolation between ambient pressure and the Thomas-Fermi limit, which leads to the use of the parameters $p_{FG}=a_{FG}(Z/V)^{5/3}$ for the Fermi-gas pressure of a solid with Z electrons in the volume V_0 with $a_{FG}=23.37$ MPa nm^5. Since the value for K_0 of Sm(I) at ambient conditions is already determined with reasonable accuracy from lower-pressure systematics,[30] the prefixed value $K_0=33(2)$ GPa was used in an attempt to determine the parameter K_0' by means of these three forms in the present least-squares fitting procedure, using all the available data, however, with five times stronger weight for the few data points of the phase Sm(VI).

In all these three attempts with second-order forms, systematic deviations exist and the standard deviations in volume ϵ_v remained larger than 4.2% which corresponds to a significant deviation. Only a third-order form $BE3$ resulted in a good fit as shown in Fig. 3 with values for $\epsilon_v=1.2\%$, $K_0'=1.7(2)$, and $-K_0K_0''=6.9(2)$, whereby the statistical errors (in brackets) for K_0' and K_0'' are almost an order of magnitude smaller than the real experimental uncertainties due to the correlations in these parameters. The small value for K_0' can here be taken as an indication for anomalous compressional behavior and, in this case, the superior fit of the form $BE3$ in comparison with the other third-order forms such as $MV3$ or $H13$ may indicate that $BE3$ is just more flexible in representing anomalies.

The anomalies in the EOS data for the individual phases can be more readily visualized by a simple "linearization" procedure, which removes the variations at small and strong compressions in the logarithmic form

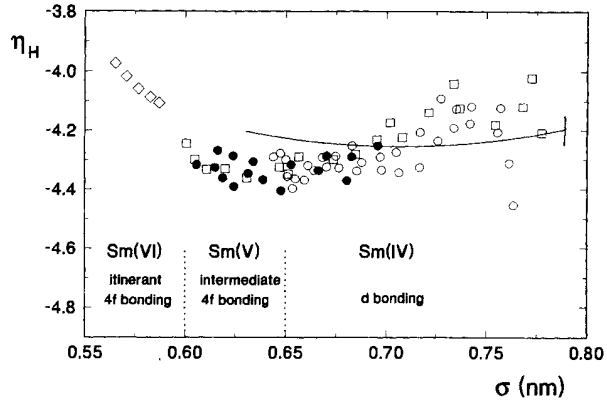

FIG. 8. Linearization of the compression data for Sm in the form of an η_H-σ plot (Ref. 29). Thereby $\eta_H=\ln(p/p_{FG})-\ln(1-\sigma/\sigma_0)$ and $\sigma=(3ZV/4\pi)^{1/3}$, where Z is the numbers of electron per atom. Solid circles are the present data. The meaning of other symbols are the same as in Fig. 3. The thin smooth curve represents the common η_H-σ relation of regular trivalent lanthanide metals (Ref. 30).

$$\eta_H=\ln(p/p_{FG})-\ln[1-(V/V_0)^{1/3}]$$

by subtraction of the last term $\ln[1-(V/V_0)^{1/3}]$ and by the scaling with the Fermi-gas pressure p_{FG} in the first term, respectively. In fact, this scaling has been applied in many recent publications[7,29–33] to distinguish between "normal" behavior of many simple metals and specific anomalies, typically related to either an *s-d* transfer in heavy alkali, earth alkali, and rare-earth metals under pressure, or to the *f*-electron delocalization in lanthanide and actinide metals.[7,30,32,33] With the present data for the intermediate phases Sm(IV) and Sm(V), Fig. 9 shows now indeed some significant anomalies just in the region of the phases Sm(IV) to Sm(VI) with respect to the smooth curve which represents the common behavior of all the other "regular" lanthanides discussed in previous publications.[7,30,32]

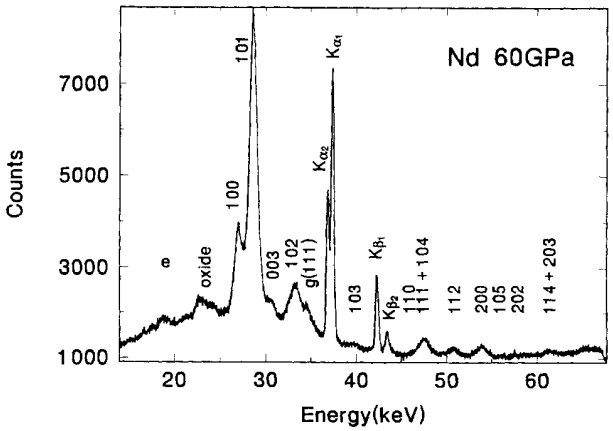

FIG. 9. Diffraction spectrum of $hP3$-type structure Nd(IV) in Nd at 60 GPa.

In fact, the anomalies of $tI2$-Sm(VI) can be related, according to a recent theoretical study,[34] to the formation of strong hybridized $4f$ bonds, however, no such calculations were performed for the intermediate phases Sm(IV) and Sm(V) due to the lack of structural data. Thus, the inspection of Fig. 8 may illustrate, that the anomalies due to the $4f$ delocalization start already in the region of the phase Sm(V) with a minor precursor possibly in the phase Sm(IV) which corresponds from the point of view of a regular structural sequence still to the region of "regular" trivalent lanthanide metals, where the (localized) $4f$ electrons make only very minor contributions to structural and bonding properties.

The same $hP3$-Sm(V)-type structure, $hP3$-Nd(IV), has also been observed in the Sm neighboring element Nd under pressure from 40 to 65 GPa. One typical diffraction spectrum for Nd at 60 GPa is shown in Fig. 9. The occurrence of this phase has also been noted at about 40 GPa in the earlier measurements up to 43 GPa, but phase mixing precluded a definite structural proposal.[14] One may conclude now by analogy that the $4f$ delocalization starts in Nd also with the transition to this "low-symmetry" structure $hP3$-Nd(IV) and further transitions, for instance into a $tI2$ structure as in Sm(VI), appear to be very likely at slightly higher pressures.

V. CONCLUSION

The crystal structure for the low-symmetry phase Sm(V) was studied by synchrotron x-ray diffraction under isothermal compression at room temperature up to 77 GPa (volume fraction=0.45). The measured lattice spacings and intensities in the pressure range beyond the phase mixing show that $hP3$-Sm(V), present from 37 to 77 GPa, is a prototype structure for elemental metals with three atoms in the hexagonal unit cell. The present study supports the view that this phase is stabilized by $4f$ bonding and is a likely candidate also for other lanthanide metals at intermediate pressures, where the $4f$ delocalization starts to continuously increase.

ACKNOWLEDGMENTS

Y.C.Z. is indebted to Alexander von Humboldt-Stiftung for financial aid. This work is supported in parts by the Bundesministerium für Forschung und Technologie (BMFT) under Contract No. 055PPAXB for DESY VI. The authors would like to thank especially Professor K. A. Gschneidner, Jr., for providing the sample material and Dr. J. Otto at the EDX station of HASYLAB for his cooperation.

*Permanent address: Beijing Synchrotron Radiation Facility, Institute of High Energy of Physics, P.O. Box 918, 100039 Beijing, China.

[1]A. Jayaraman, Phys. Rev. A **135**, 1056 (1964).
[2]D. B. McWhan, Science **176**, 75 (1972).
[3]K. A. Gschneidner, Jr. and F. W. Calderwood, in *Handbook on the Physics and Chemistry of Rare Earths,* edited by K. A. Gschneidner, Jr. and L. Eyring (North-Holland, Amsterdam, 1986), Vol. 8, p. 1.
[4]U. Benedict, W. A. Grosshans, and W. B. Holzapfel, Physica **144B**, 14 (1986).
[5]W. A. Grosshans, Ph.D. thesis, University of Paderborn, 1987.
[6]T. Krüger, B. Merkau, W. A. Grosshans, and W. B. Holzapfel, High Press. Res. **2**, 193 (1990).
[7]U. Benedict and W. B. Holzapfel, in *Lanthanides/Actinides; Physics I,* Handbook on the Physics and Chemistry of Rare Earths Vol. 17, edited by K. A. Gschneidner, Jr., L. Eyring, G. H. Lander, and G. R. Choppin (North-Holland, Amsterdam, 1993), p. 245.
[8]J. C. Duthie and D. G. Pettifor, Phys. Rev. Lett. **38**, 564 (1977).
[9]H. L. Skriver, Phys. Rev. Lett. **49**, 1768 (1982); Phys. Rev. B **31**, 1909 (1985).
[10]*Nomenclature of Inorganic Chemistry, Recommendations 1990,* edited by G. J. Leigh (Blackwell Scientific, Oxford, London, 1990).
[11]N. Hamaya, Y. Sakamoto, H. Fujihisa, Y. Fujii, K. Takemura, T. Kikegawa, and O. Shimomura, J. Phys. Condens. Matter **5**, L369 (1993).
[12]S. Endo, N. Fujioka, and H. Sasaki, J. Phys. Soc. Jpn. **42**, 882 (1977).
[13]W. A. Grosshans, Y. K. Vohra, and W. B. Holzapfel, J. Phys. F **13**, L147 (1983).
[14]W. A. Grosshans and W. B. Holzapfel, J. Phys. (Paris) Colloq. **45**, C8-141 (1984).
[15]J. Staun Olsen, S. Steenstrup, L. Gerward, U. Benedict, J. Akella, and G. Smith, High Press. Res. **4**, 366 (1990).
[16]Y. Vohra, L. Akella, S. Weir, and G. A. Smith, Phys. Lett. A **158**, 89 (1991).
[17]W. A. Grosshans, E.-F. Düsinger, and W. B. Holzapfel, High Temp. High Pressure **16**, 539 (1984).
[18]K. Syassen and W. B. Holzapfel, Europhys. Conf. Abstr. **1A**, 75 (1975).
[19]W. B. Holzapfel, in *High Pressure Chemistry,* edited by H. Kelm (Reidel, Boston, 1978), p. 177.
[20]H. K. Mao, P. M. Bell, J. W. Shaner, and D. J. Steinberg, J. Appl. Phys. **49**, 3276 (1978).
[21]F. Porsch and W. B. Holzapfel (unpublished).
[22]R. Keller, W. B. Holzapfel, and H. Schulz, Phys. Rev. B **16**, 4404 (1977).
[23]J. C. Tolédano and P. Tolédano, Phys. Rev. B **21**, 1139 (1980).
[24]M. H. B. Ghozlen and Y. Mlik, J. Phys. C **16**, 4365 (1983).
[25]F. Porsch and W. B. Holzapfel, Phys. Rev. Lett. **70**, 4087 (1993).
[26]W. B. Holzapfel, in *Molecular Solids under Pressure,* edited by R. Pucci and G. Piccitto (North-Holland, Amsterdam, 1991), p. 61.
[27]F. Birch, J. Geophys. Res. **57**, 227 (1952).
[28]P. Vinet, J. Ferrante, H. Rose, and J. R. Smith, J. Geophys. Res. **92**, 9319 (1987).
[29]W. B. Holzapfel, Europhys. Lett. **16**, 67 (1991).
[30]W. B. Holzapfel, Physica B **190**, 21 (1993).
[31]O. Schulte and W. B. Holzapfel, Phys. Rev. B **48**, 767 (1993).
[32]W. A. Grosshans and W. B. Holzapfel, Phys. Rev. B **45**, 5171 (1992).
[33]Y. K. Vohra and W. B. Holzapfel, High Press. Res. **11**, 223 (1992).
[34]P. Söderlind, O. Eriksson, J. M. Wills, and B. Johansson, Phys. Rev. B **48**, 9212 (1993).

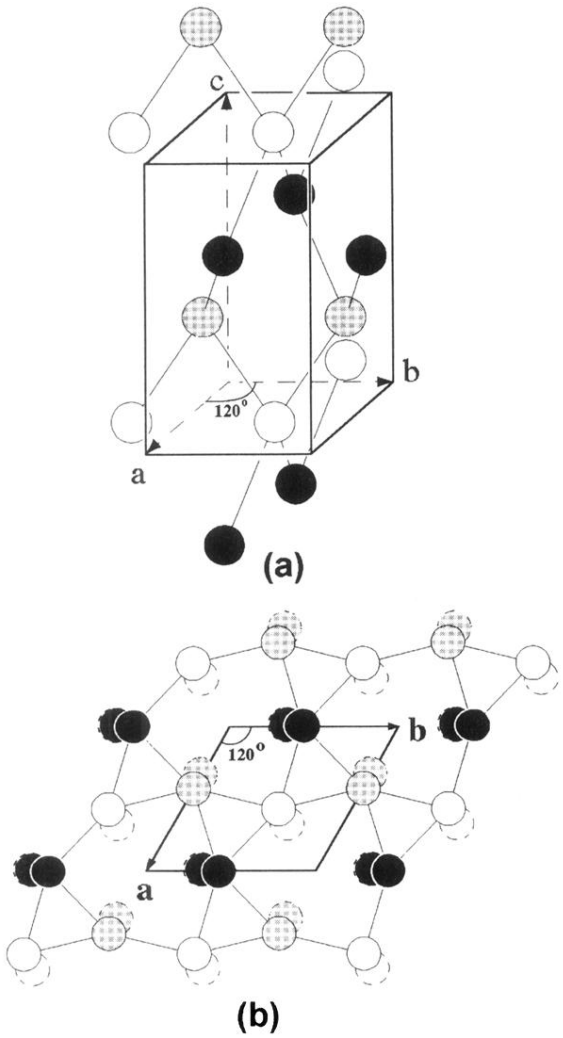

FIG. 6. Crystal structure of Sm(V) (a) and atomic arrangement projected along the c axis (b). White, gray, and black balls represent $z=0$, $\frac{1}{3}$, and $\frac{2}{3}$, respectively. In (b) the balls with dashed rim represent the fcc positions. The hexagonal unit cell is represented by thick lines and the bonds among the nearest neighbors are shown by thin lines.